

The impact of Atlantic and Pacific Ocean sea surface temperature anomalies on the North Atlantic multidecadal variability

By Klaus Grosfeld*, Gerrit Lohmann and Norel Rimbu

Alfred Wegener Institute for Polar and Marine Research, Bussestraße 24, 27570 Bremerhaven, Germany

(Manuscript received ...)

ABSTRACT

Globally forced model simulations with an atmospheric general circulation model of intermediate complexity reveal surface air temperature (SAT) and sea level pressure (SLP) variations at multidecadal time scales. In order to separate the influence of individual ocean basins on the North Atlantic multidecadal variability, we force our model with observed SST data for the period 1856–2000 for Atlantic and Pacific Oceans, separately, while outside the atmosphere is coupled with the ocean via a mixed layer slab model. The experiments indicate the Atlantic Ocean as a principal driver of North Atlantic multidecadal variability, with SAT and SLP highly in phase in the North Atlantic at about 60–70 years time scale. The Pacific impact is associated to longer period variations in the SLP field over the North Atlantic. We suggest that two distinct physical modes of multidecadal climate variability exist, one of about 70 years possibly linked with the Atlantic thermohaline circulation, the other linked with the Pacific Ocean and connected to the Atlantic Ocean via Pacific - North America teleconnections. The latter has a time scale of about 80–100 years.

1 Introduction

During the 20th century, climate in the North Atlantic realm experienced pronounced multidecadal variations. An abrupt transition from relatively cold to relatively warm conditions occurred in the 1930s (Minobe, 1997). The relatively warm conditions dominated the North Atlantic climate several decades, until the system jumped back to relatively cold conditions in 1970s. The latter regime change is strongly correlated with the Great Salinity Anomaly in the North Atlantic (Dickson et al., 1988). The cold regime induces an enhancement of the mean mid-latitude westerly flow, leading to a warming of the Euro-Atlantic sector (Thompson et al., 2000) with corresponding impact on the hydrology (e.g. Hurrell, 1996) and terrestrial ecosystems (e.g. Stenseth et al., 1999). The atmospheric counterpart to such like sea surface temperature (SST) changes consists of a negative (positive) sea level pressure (SLP) anomaly over Iceland and northwestern Europe during cold (warm) SSTs as well as positive (negative) SLP anomalies over southwestern and central North Atlantic and Europe (Delworth and Mann, 2000).

On interannual to decadal time scales, the 1970s regime shift goes along with a change in the North Atlantic Oscillation (NAO) (Hurrell, 1995), depicting a transition from its negative to positive phase. It has been argued, that these changes are part of a long-term multidecadal climate

variation, as suggested from analysis of instrumental and proxy data (e.g. Deser and Blackmon, 1993; Kushnir, 1994; Schlesinger and Ramankutty, 1994; Mann and Park, 1999; Delworth and Mann, 2000; Gray et al., 2003). The variation at multidecadal time scales has been termed Atlantic Multidecadal Oscillation (AMO) (e.g. Kerr, 2000). While the phenomenon was already discussed by Bjerknes (1964), AMO was first defined by Enfield et al. (2001) who argued that the SST from the North Atlantic ocean follows a quasi-periodic cycle. During the extreme phases, the entire North Atlantic ocean is dominated by mono-polar SST anomalies with significant climatic anomalies over the North American continent (Enfield et al., 2001) and teleconnections to the North Pacific (Minobe, 1997). Recently, Dima and Lohmann (2007) proposed a deterministic frame, in which the Atlantic thermohaline circulation, sea-ice and freshwater export from the Arctic, and atmospheric dynamics represent a memory and a negative feedback as necessary elements for the generation of the quasi-periodic multidecadal mode. A similar mechanism was suggested by Jungclaus et al. (2005) who analysed a 500-yr model integration of a coupled atmosphere-sea ice-ocean model. They found pronounced multidecadal fluctuations of the Atlantic meridional overturning circulation and the associated net flux with periods of 70–80 years, which correlates to convection activity in deep-water formation regions and fresh water exports from the Arctic.

On decadal time scales a relation between the low-frequency change of the NAO and SST variability was found by Rodwell et al. (1999), Latif et al. (2000), and Mehta et al. (2000) from atmospheric general circulation model (AGCM)

* Corresponding author.
e-mail: Klaus.Grosfeld@awi.de

experiments forced with observed SST and sea ice concentration data over the last 50 years. Their results indicate that the atmospheric response, e.g. the SLP pattern over North Atlantic, is predictable as long the SST is predictable. North Atlantic climate variability is therefore not merely stochastic noise or result of internal atmospheric variability (James and James, 1989; Saravanan and McWilliams, 2001).

Numerical simulations forced with the latest version of the Global Sea Ice and Sea Surface Temperature (GISST) data set by Sutton and Hodson (2003), indicate a close correlation between Atlantic SST variability and NAO with impacts from other ocean basins. Applying a new global climate model, Latif et al. (2004) showed that multidecadal SST variability of the North Atlantic is closely related to the thermohaline circulation, exhibiting a relatively high degree of predictability at decadal time scales derived from control and anthropogenically forced simulation experiments.

Despite the finding that on multidecadal time scales the oceanic influence on the NAO encompasses the whole North Atlantic (Sutton and Hodson, 2003) and can be attributed to the North Atlantic thermohaline circulation (Pohlmann et al., 2004), the key questions about interbasin impacts and different origins of North Atlantic climate variability remain. Especially, a tropical link relating warming processes of the tropical ocean with the NAO (Hoerling et al., 2001; Bader and Latif, 2003) comes into the focus. Pohlmann and Latif (2005) found that both, Atlantic and Indo-Pacific oceans are important for the generation of the SLP variability in the North Atlantic with Indo-Pacific forcing projecting on the NAO. Furthermore, El Niño Southern Oscillation (ENSO) teleconnection patterns are modulated on multidecadal time scales affecting the climate in the Euro-Atlantic realm (Rimbu et al., 2003; Greatbatch and Peterson, 2004). Lohmann et al. (2004) analyzed possible origins of the Atlantic AMO from observational and proxy data and found solar irradiance and Atlantic ocean circulation changes as two dominating modes of the multidecadal variability. In a recent study Zhang et al. (2007) showed from forced climate model studies that Atlantic multidecadal variability could play an important role in the non-monotonic Northern Hemisphere temperature evolution during the 20th century.

In our study we concentrate on multidecadal climate variations in the Atlantic region and decompose the AMO signature over observational period 1856 to 2000 in relation to different ocean basin source regions. This is done by prescribing the SST forcing in different ocean basins and allowing the SST outside to evolve freely. Analyses of the climate feedback on different forcing fields provide insights into the relative role of different ocean basins on the atmospheric multidecadal mode.

The paper is organized as follows: the model concept and the experimental setup are introduced in Section 2. Results from different model experiments are presented in Section 3 and discussed in Section 4. Conclusions are drawn in Section 5.

2 Model experiments and setup

We use the Portable University Model of the Atmosphere (PUMA), Version 2, developed at the University of Hamburg (Fraedrich et al., 1998; 2005). PUMA belongs to

models of medium complexity (Claussen et al., 2002) and, therefore, is suitable for long-term climate variability simulations. It is derived from the Reading multi-level spectral model described by Hoskins and Simmons (1975). While the moist primitive equations are numerically integrated in terms of the vertical component of absolute vorticity, the horizontal divergence, the temperature, the logarithm of the surface pressure and the specific humidity, surface fluxes of moisture, heat and momentum are based on bulk formulas. The radiation uses a one band approximation for the long wave part and a two band approximation for the short wave part. Large scale precipitation for super-saturated air and a Kuo type convective precipitation scheme (Kuo, 1965; 1974) complete the atmospheric water cycle. Clouds are formed diagnostically based on the relative humidity. In the present study, PUMA is integrated in T-21 spectral resolution, corresponding to Gaussian grid of 5.625° in longitude and 5.625° in latitude. Five equally spaced, terrain following sigma-levels are used in the vertical. The land temperatures, soil hydrography and river runoff are parameterized in the model. A detailed description of model design, setup is given by Romanova et al. (2006), an intercomparison to AGCM ECHAM4 results is given in Grosfeld et al. (2007).

The model studies are performed in an ensemble mode with 20 ensemble members for each experiment. The initial conditions of the ensemble members are chosen at different states (19 different years from 1857 to 1875) of the results derived from the initial model run which started from atmosphere at rest. The influence of the 145 years variability of CO₂ concentration and of solar irradiance has been investigated in a separate model run with climatological SST forcing over the whole 145 years period and has found to be small compared to the simulations forced with observed SST data. Because the SST variability captures most of the climate forcing and the atmosphere is mainly heated from below, CO₂ concentration of the atmosphere and solar irradiance is set constant to present day conditions over the whole integration period.

As forcing data, an updated (1856-2000) version of the Kaplan et al. (1998) monthly global SST anomalies is taken superposed onto the global SST climatology given by the Hadley Centre for Climate Prediction and Research (Rayner et al., 1996). Different experiments where SST forcing is restricted to different ocean basins Atlantic or Pacific Oceans are performed. In the remaining ocean basins, PUMA is coupled to a mixed layer slab-ocean model with 50 m depth (Romanova et al., 2006). The mixed layer temperature is calculated from atmospheric heat fluxes, provided by the AGCM, and prescribed monthly oceanic heat fluxes. The latter are diagnosed from a model experiment where PUMA is forced with climatological SST data (Rayner et al., 1996) for 50 years. In this area, the SST is solely determined by climatological oceanic heat flux and by atmospheric teleconnections from the other basins.

The following integrations are performed: As control experiment (GLOB), PUMA is forced with 145 years of global SST variability (Rayner et al., 1996; Kaplan et al., 1998). In experiments ATL and PAC, PUMA is forced with SST variability in Atlantic and Pacific Oceans, respectively, while outside the mixed layer slab ocean is applied. The boundaries between the different basins are given in longitude with the southern tips of South-America, Africa, and Australia,

and in latitude with the continental margins. The North Atlantic is limited to the North at 75°N (see Fig. 1). All experiments were integrated in a 20-ensemble set, each.

3 Results

3.1 Global SST forcing

3.1.1 Identifying the multidecadal mode In order to evaluate the global atmospheric variability for 145-years integration of PUMA forced with global SST GLOB and for comparison with later ATL and PAC experiments, we applied a global empirical orthogonal function (EOF) analysis (e.g. von Storch and Zwiers, 1999) of the ensemble mean surface air temperature (SAT) for boreal winter. Prior to the analysis, the data are normalized to unit variance by their temporal standard deviation. The linear trend was subtracted, and a 21-year running mean filter was applied to the time series of boreal winter means to capture predominantly the multidecadal signal. In our study we concentrate on boreal winter data (December, January, February) because atmospheric teleconnections are strongest during this season.

The first EOF of linear detrended simulated SAT data (Fig. 2a), explaining 37% of the variance, depicts alternating bands of changing amplitudes in the Pacific Ocean as well as in several regions of the Atlantic and Indian Oceans. The second EOF of global SAT explains 22% of the variance (Fig. 2b). It shows an interhemispheric seesaw pattern over the Atlantic, indicative for multidecadal fluctuations of the Atlantic thermohaline circulation (e.g. Crowley, 1992; Delworth and Mann, 2000). Similar patterns of Atlantic multidecadal variations were identified in various observational and modeling studies (e.g. Deser and Blackmon, 1993; Delworth and Mann, 2000; Knight et al., 2005). The principal components (PC) associated with the first (second) SAT pattern has a time scale of about 100 years (70 years) (Fig. 2c).

The analysis of the detrended data (Fig. 2a,b,c) masks the impact of the dominating climate signal of the industrial period, the global warming signal based on anthropogenic forcing. To separate our analysis of the multidecadal mode from the dominating pattern, we also show an analysis of global SAT of the non-detrended fields. The resulting PC1 (Fig. 2f) of the non-detrended SAT field shows a strong trend between 1910 and 1940, and 1970 and 2000, interrupted by stagnation between 1940 and 1970. In this respect, PC1 is similar to the time series of the global mean temperature of observational period (e.g. Folland et al., 2001, Figure 2.6) and resembles the impact of variation in external forcing (greenhouse gases, aerosol and solar irradiance). Beside the trend, the general characteristic of PC1 based on detrended and non-detrended data is similar, namely the local maximum between 1870 and 1900 and the strong temperature increase after 1970. In between, the time series is interrupted by an undulation/plateau, where the North Atlantic Ocean experienced a cooling phase (IPCC, 2001). The associated EOF1 of the SAT field (Fig. 2d) explains 60% of the variance instead of 37% in the detrended field. The detrended and non-detrended patterns are similar in the Pacific but differ in the North Atlantic, where the negative anomaly is confined to the northern North Atlantic. PC2 and the asso-

ciated patterns of both analyses are quite similar; the non-detrended data explains 15% of the variance instead of 22% based on detrended data. In the detrended version, EOF1 resembles the atmospheric response pattern on climate forcing that is possibly associated with the multidecadal variations rather than the pattern that is dominated by anthropogenic forcing as revealed in the long term trend. In order to mask out the dominant signal of the climate warming trend, all following analyses are, therefore, based on linear detrended data.

3.1.2 North Atlantic mean SAT and SLP signature The mean model response with respect to multidecadal variability is quantified with a temperature index over the region (60°W – 0°W, 0°N – 60°N) in the North Atlantic, representing the large-area mono-polar SAT pattern (Fig. 3a). Prior to the analysis the data was detrended, filtered with a running mean over 21 years, and centered around its long term mean. Warm phases (1875–1895, 1930–1965 and 1995 onward) as well as cold phases (1900–1930 and 1960–1990) are clearly emphasized in North Atlantic SAT from each ensemble member. The ensemble mean index is highly correlated ($r=0.93$) with PC2 from the global EOF. An increase in temperature during the last decade of the 20th century is realized in almost all ensemble members. The variability within the ensemble is small and the multidecadal temperature signal with a period of about 70 years is detected in each member (Fig. 3a). Multidecadal variations at 70 -years scale are clearly seen in unfiltered time series of the ensemble mean (Fig. 3c). For a statistical analysis of the ensemble simulations, we refer to the appendix. In addition, two independent time series of the North Atlantic mean SST as derived from the Mann et al. (1998) and Kaplan et al. (1998) data sets are shown in Fig. 3c. The different time series show generally good agreement, only the amplitude range is higher in the observations because of the slightly different data sets: SST in observations instead of SAT in the model output.

On multidecadal time scales, the mono-polar SST pattern in the North Atlantic is in our simulation associated with a mono-polar SLP pattern (Fig. 4). Based on this pattern, we define an SLP index by averaging the SLP anomaly over the area between 60°W – 0°W and 0°N – 60°N. The corresponding indices for the ensemble members together with the ensemble mean are shown in Fig. 3b. The variability between the ensemble members is higher than for SAT. A clear maximum from 1885 – 1915 and after 1975 is detected. It is halted by a distinct minimum between 1920 and 1970. The long term variation of the index displays a longer period of about 90 years compared to the SAT index. The multidecadal variation is evident also in the unfiltered time series of the SLP index averaged within the ensemble members (Fig. 3d). Hence, the SLP field over the North Atlantic is obviously influenced by other mechanisms than purely Atlantic SST forcing. Comparison with observational data and reconstructions by Kaplan et al. (2000) and Luterbacher et al. (2002) indicates a slight phase shift of the local maximum from 1900 to 1920. The amplitude range is also stronger than in the modeled SLP field. Nevertheless, the general structure of a long term SLP variation with longer period than in SAT is prevailed.

The choice of the index region for SLP and the impact of possible local SLP forcing can be validated by regressing the non-normalized SLP anomaly field against the SAT index. Fig. 4 indicates a mono-polar SLP pattern in the North Atlantic with a local maximum at the east American coast. The chosen SLP index region (described above) is not influenced by local variability, especially no sign change occurs here. The amplitude is between -0.1 hPa and -0.2 hPa and covers the range found in Fig. 3c. Hence, the derived SLP index is not very sensitive to the chosen index region, which was also confirmed by analyses performed on varying index regions (not shown).

3.1.3 Canonical correlation analysis In order to investigate the connection between SAT and SLP fields in experiment GLOB, we performed a canonical correlation analysis (CCA) (e.g. von Storch and Zwiers, 1999) to the global SAT and SLP fields. CCA is a multivariate statistical analysis technique exploring the linear relation between two sets of space-time dependent variables. By this method, the data are decomposed into pairs of spatial patterns in such a way that their time series are optimally correlated. The CCA was performed with the simulated global SAT and SLP fields covering the observational period from 1856 to 2000. Only the first four EOFs of SAT and SLP fields were retained for the CCAs. They explain 84.6% (SAT) and 81.8% (SLP) of the field variance. The first canonical mode (Fig. 5b) explains 24.8% of the variance in the SAT field and 34.4% of the variance in the SLP field (Fig. 5c). By construction, the correlation coefficients between the corresponding time series is high (0.99) (Fig. 5a). The SAT mode (Fig. 5b) displays strong negative amplitudes in the North Atlantic and north-west Eurasia, while in the Pacific realm, the tropics and the Alaska region show high positive values. This pattern is supported in the field of locally explained variance (grey shading in Fig. 5b). High values of explained variance are found in the equatorial Pacific (80%), in the Alaska and Barents Sea region. The SLP mode (Fig. 5c) shows high amplitudes over North America and alternating bands over the Pacific with explained variances exceeding 80%. Again, high values are found in the equatorial Pacific. The time series (Fig. 5a) of the first canonical mode depicts multidecadal variability at about 90 years period, with a clear maximum from 1890 – 1910 and after 1980, similar to the time series of the first EOF of the detrended SAT field (Fig. 2c) and to the SLP index of the North Atlantic (Fig. 3b). In order to quantify more detailed the response of the free atmosphere we analyse the vertical structure of the atmosphere in terms of geopotential height at 500 hPa (GPH500). In Fig. 5d,e,f the results of a CCA between SAT and GPH500 is shown, explaining 84.7% and 84.8% of the SAT and SLP fields variance, respectively. The time series (Fig. 5d) of the first canonical mode indicates similar variation at multidecadal time scale of about 90 years and a comparable SAT mode (Fig. 5e) as the previous analysis. In GPH500, highest amplitudes are found over Eurasia and in the Aleutian region, with explained variances exceeding 80%, locally. In the subtropical North Pacific a PNA-like structure arises, connecting probably Pacific and Atlantic multidecadal variations.

3.2 Atlantic Ocean SST forcing

3.2.1 Identifying the multidecadal mode To decompose the global pattern on multidecadal time scales and to investigate possible links of the AMO with separate ocean basins, we performed two sets of ensemble experiments, where different ocean basins are forced with SST variability and outside a mixed layer slab ocean forced with climatological heat flux is applied. PC1 for experiment ATL (Fig. 6a) shows the same periodicity as PC2 for experiment GLOB (Fig. 2c) ($r=0.92$). The corresponding EOF (Fig. 7b), which explains 43% of the variance, is similar to EOF2 in experiment GLOB in the Atlantic Ocean. Outside the Atlantic, the applied mixed layer with climatological heat flux forcing leads to a different SAT pattern than the second EOF in experiment GLOB. The setup induces a Pacific SAT pattern of high variability especially in the region of the Aleutian Low. The extension of the North Atlantic mono-polar signal to the eastern equatorial Pacific indicates the impact of the Atlantic onto the Pacific Ocean which, however, is too weak to be detected in the globally forced experiment (Fig. 2). The Pacific Ocean pattern is dominated by SST variability of the Pacific Ocean itself.

3.2.2 Canonical correlation analysis The time series obtained from CCA between the SAT and SLP fields are highly correlated (0.99) and are presented in Fig. 7a. Multidecadal variability is conspicuous with a period of about 60-70 years. The associated modes explain 71.7% of the SAT field and 67.9% of the SLP field, respectively, based upon the first four EOFs. The first SAT mode (explaining 31.8% of the total variance) shows expected high values over entire North Atlantic for SAT with highest values in the tropics similar to the first EOF (Fig. 7b). Only near the North American coast, where land temperatures have large influence on the ocean, the CCA shows lower values. The local explained variance (Fig. 7b, grey shading) exceeds 90% in the tropical Atlantic and high values overall Atlantic. Some connections to the equatorial Pacific are seen, indicating a possible AMO impact on that region. High values of the SAT mode are also found over entire Eurasian continent with amplitudes of local explained variance up to 90% in the eastern Mediterranean and Himalaya regions. The SLP mode (33.7%) (Fig. 7c) emphasizes a seesaw between the Atlantic and Pacific oceans. The warm phase of North Atlantic is related to low pressure over the entire North Atlantic and a high pressure field over equatorial and North Pacific, indicating a lowering of the Azores High and a weakening (increase in pressure) of the Aleutian Low. Highest values are found in the tropics, especially in the west Pacific warm pool, indicating teleconnections of the North Atlantic multidecadal variability on this region, probably via the North Pacific. The highest values of the locally explained variance (Fig. 7c, grey shading) is concentrated in the tropical Atlantic (90%), the west Pacific warm pool (80%), and the western and eastern North Pacific (80%). Again, largest values of explained variance are found in the eastern Mediterranean.

The CCA analysis between SAT and GPH500 explains 71.7% of the SAT field and 77.9% of the GPH500 field. The first SAT mode explains 30.4% of the total variance and is nearly identical to the CCA analysis with SLP. The GPH500 mode (44.2%) shows high amplitudes in the tropics and the

northern North Pacific with local explained variance of up to 90%. The local minimum in western Pacific correlates in SLP and GPH500 fields, indicative for a barotropic signal. Negative pressure anomalies over North American continent in GPH500 are extended in SLP over the entire North Atlantic and Eurasia, indicating the west-east seesaw. Over the southern ocean both modes are identical.

Based on the CCA SLP pattern (Fig. 7c), we defined an index as difference between the mean SLP of the entire North Atlantic and the entire North Pacific. This index (Fig. 7a, dashed-dotted line) is highly correlated with the time series of the first CCA modes, indicating a strong connection of the SLP fields in the Atlantic and Pacific Oceans at multidecadal time scales. Analogue to the globally forced model runs (Fig. 3) we calculate SAT and SLP indices, based on CCA results and regions with high values of explained variance. The index region for SAT covers the whole North Atlantic and shows clear multidecadal variations at about 60-70 years period (Fig. 8a), similar to the GLOB temperature index (Fig. 3a). The corresponding SLP index (Fig. 8b) is different than for GLOB, showing the same variation as for SAT but in opposite phase. The correlation coefficient between the ATL ensemble mean indices of SAT and SLP is calculated to be $r=-0.84$. Regression of the calculated indices with the non-normalized ensemble mean SAT and SLP patterns indicate clear mono-polar basin-wide patterns over North Atlantic (Fig. 8c), and a pronounced inter-ocean seesaw in SLP with amplitude maxima in the central North Atlantic and northwest Pacific (Fig. 8d). In the SAT pattern (Fig. 8c) the Atlantic mono-polar signal reaches about 1.2°C but is almost stronger over central Europe. The corresponding SLP pattern depicts an extension of positive anomalous pressure over Europe.

3.3 Pacific Ocean SST forcing

3.3.1 Identifying the multidecadal mode For the Pacific Ocean forcing experiment (PAC), PC1 shows multidecadal variability with a dominant period of about 80-100 years (Fig. 9), similar to PC1 of experiment GLOB (Fig. 2c), with a more pronounced local maximum around 1940. In the non-detrended field, the EOF (not shown) yields the same pattern in the first mode, explaining 61% of the local variance regarding mainly the impact of the warming trend. In the detrended field (Fig. 9b), the first EOF explains 53% of the variance. In Pacific and Indian Oceans it has a similar but not the same structure as the first EOF in experiment GLOB (Fig. 2a), suggesting lacking teleconnections and/or forcing within the Atlantic Ocean. Over the Atlantic a seesaw establishes. The negative anomaly in the north-western North Atlantic is highly correlated with the pattern of the non-detrended SAT field of experiment GLOB, but with reduced amplitude. This means that teleconnections within the Atlantic and/or local forcing are important contributors to the global atmospheric circulation regime on multidecadal time scales.

3.3.2 Canonical correlation analysis Performing a CCA analysis of the SAT and SLP fields for experiment PAC, the time series of the canonical mode show also highly correlated (0.99) multidecadal variations at about 80-90

years period (Fig. 10a). The time series are very similar to the corresponding time series of experiment GLOB ($r=0.91$), suggesting the Pacific Ocean as an important source region for the AMO. The associated first four canonical modes of SAT and SLP explain 81.3% and 69.7% of the total variance, respectively. The first SAT mode (23.5%) (Fig. 10b) shows high amplitudes with explained variance of more than 80% in the equatorial Pacific region (Fig. 10d). This pattern reflects mainly the anomalous warm (El Niño-like) conditions during the early and late 20th century and anomalous cold (La Niña-like) conditions between 1940 and 1970. There is evidence for a tropical link to positive values in the Indian Ocean and in the tropical Atlantic. A calculated Niño3 index of the ensemble mean SAT pattern depicts a clear multidecadal to centennial signal at about 83 years period (in phase with PNA-like index and CCA time series) with high frequency modulations at decadal time scale (Fig. 10a, dashed-dotted line). The first SLP mode (Fig. 10c) suggests a coherent impact of Pacific SST variability on the North Atlantic at multidecadal time scales. The SLP field (20.9%) depicts a Pacific-North American (PNA)-like structure in its positive phase with warm conditions in the tropical Pacific. A center of high correlation values is located over entire North America (although explaining about 50% of the local variance) and extending to the western tropical Atlantic (explained local variance of 80%), indicating a teleconnection bridge between Pacific and Atlantic Oceans. Additional centers, seen in the field of explained variance of the CCA analysis (Fig. 10c, grey shading), stand out in the equatorial and central Pacific and in the North Atlantic. Calculating a PNA-like index, according to the regions given by Wallace and Gutzler (1981) ($(20^{\circ}\text{N}, 160^{\circ}\text{W}), (45^{\circ}\text{N}, 165^{\circ}\text{W}), (55^{\circ}\text{N}, 115^{\circ}\text{W}), (30^{\circ}\text{N}, 85^{\circ}\text{W})$) but adapted to the result of the CCA analysis, a clear multidecadal variation can be derived (Fig. 10a, dotted line), which highly correlates with the time series of the first CCA mode.

The corresponding CCA analysis of SAT and GPH500 fields explains 82.6% and 80.9% of the variance. The first mode in SAT shows again a similar pattern to the SAT-SLP CCA seesaw over the Atlantic and high amplitudes in the equatorial Pacific. In the GPH500 field (10.2%), a clear PNA-like structure can be seen, although with locally only 60% of explained variance in the eastern Pacific and lower values elsewhere. This might be a result of the experimental setup, with climatological forces mixed layer outside the Pacific Ocean, damping the feedback of the Pacific induced signal. The time series of the CCA analysis shows a similar variation as for SAT-SLP, but with reduced amplitudes between 1970 and 1990.

Over the North Atlantic, a negative pressure anomaly in CCA1 is flanked by a positive anomaly extending over the North American continent. This pressure system induces cold winds from the northwest, leading to a cooling of the ocean, as seen in the corresponding CCA1 of SAT (Fig. 10b). The dipolar pressure anomaly in CCA1 over the North Atlantic prohibits an index calculation of mean SLP over the entire ocean. Hence, we choose the region of high values of explained variance in the western tropical Atlantic, yielding a multidecadal variation of the calculated index (Fig. 11b) similar to experiment GLOB (Fig. 3b). In experiment PAC, the Atlantic index is a result of teleconnections only,

rather than of SST forcing as it is the case in experiments ATL and GLOB. Therefore, the spread and, hence, the variation of each ensemble member is expected to be higher in experiment PAC. The general longterm variation is included in each ensemble member, anyhow. The corresponding SAT index (Fig. 11a, also calculated in the western tropical Atlantic) exhibits the same variation as SLP but in opposite phase. The regression analysis of these two indices with non-normalized PAC ensemble mean data (Fig. 11c,d) shows high values in the index regions and a clear PNA-like structure in the SLP field. The sign change in the SAT field (compared to CCA1 in Fig. 10a) comes from the SAT index, which is in opposite phase to the SLP index. Regarding the fact that the indexing region in experiment PAC is different than for experiments GLOB and ATL, we calculate the same index for these experiments, but based on the new index regions. Fig. 12 shows that new SLP indices in GLOB and PAC are fairly similar, while ATL depicts a shorter variation pointing to a similar forcing mechanism of the atmospheric flow systems in experiments GLOB and PAC.

4 Discussion

Based on proxy data analysis and model simulations, the AMO is argued to be a persistent climate mode with possible predictive skill, exerting influence on the Euro-Atlantic sector (e.g. Sutton and Hodson, 2003; Pohlmann et al., 2004). Performing AGCM studies including a mixed layer ocean model, our experiments aim to decompose possible source regions and distinct modes of the AMO. Despite a dominating trend in the analysis of the SAT global field, indicative for the global warming signal based on greenhouse and probably volcanic atmospheric forcing (IPCC, 2001), two modes in the multidecadal time frame are found in globally forced ensemble experiments, explaining together about 60% of the total variance after linear detrending (Fig. 2). A shorter periodicity (about 60-70 years) with origin in the Atlantic Ocean is probably connected to multidecadal fluctuations of the thermohaline circulation (Delworth and Mann, 2000; Knight et al., 2005). A longer periodicity (about 80-100 years) with origin in the Pacific Ocean is closely connected to tropical Pacific variations. A such like separation was already discussed by Lohmann et al. (2004) from observational and proxy data analyses. They associate the longer variation as possibly induced by solar irradiance, namely the Gleisberg cycle, at about the same periodicity. Their analysis was based onto detrended and normalized annual mean data given a similar pattern as compared to ours. The multidecadal mode is also captured in the Delworth and Mann (2000) proxy data analysis for reconstructed surface temperature patterns (1650-1980). With the multivariate frequency-domain method which identifies coherent oscillatory and secular modes of variance they show in their local fractional variance spectral analysis (Figure 4a in Delworth and Mann, 2000) two clearly separated, highly significant peaks above 99% confidence level, one at about 60 years and a second one at about 90 years. In conjunction with coupled ocean-atmosphere model experiments, Delworth and Mann interpreted these peaks as one centered around 70 years. In our GLOB experiment, the Atlantic Ocean indices defined for SAT and SLP also reveal two periods, a shorter about

65-years period for SAT and a longer about 90-years period for SLP variations, similar to the global EOF analysis of the modeled SAT field (Fig. 2c). According to Barsugli and Battisti (1998) and Bretherton and Battisti (2000) one could argue for a stochastic response of the atmosphere model to the SST forcing rather than a dynamical response, provoking the low-frequency response. However, as obvious from our index calculation for individual ensemble members (Fig. 3a,b), the low-frequency variation is a persistent response in all experiments, speaking for a dominating feature not induced by noise but by the SST forcing.

Ensemble experiments with SST forcing in the Atlantic Ocean and climatological heat flux forcing of a mixed layer ocean model outside the Atlantic show the Atlantic as the main driver for the AMO with a clear coherence between SAT and SLP fields. A CCA for this model experiment displays a multidecadal variation with about 60-70 years period, indicating the Atlantic component of the AMO. The SAT field depicts a mono-polar basin wide pattern superposed by a SLP seesaw between Atlantic and Pacific Oceans, a pattern that was also found by Dima and Lohmann (2007) from the EOF analyses of observed winter hemispheric SLP and from composite maps. Hence, variations in Atlantic SST may impact the Pacific via the pressure field, especially in the Northeast Pacific and Aleutian region, indicating that a purely Atlantic SST signal has a strong impact on the North Pacific pressure field, which is also evident at GPH500.

The climate warming signal after 1960 in tropical Pacific can be interpreted as part of solar irradiance forcing connected with the Gleisberg cycle on multidecadal time scales (Hoyt and Schatten, 1997). Lohmann et al. (2004) argue that an increase in SST may enhance convection and hence Walker circulation, leading to anomalous westward winds influencing the SST outside the Pacific. A link between Atlantic and eastern tropical Pacific was also found in experiments ATL (Fig. 8b). In contrast to our study, Hoerling et al. (2001) suggest that the observed warming trend, including the positive trend in the NAO-like pattern in the North Atlantic, has its origin primarily in the evolution of the tropical Indian and Pacific SST. Schneider et al. (2003), who investigated the DJF 500-hPa geopotential, however, associate the trend for the last 50 years to a forced signal in the Pacific-North American sector. The trend in the North Atlantic sector might be associated with internal atmospheric noise with annular structure (Schneider et al., 2003).

5 Concluding remarks

A pure modelling approach to investigate source regions for the Atlantic multidecadal oscillation is the only possibility to decompose this climate mode in terms of most important source regions and probable time scales of its variation. An atmospheric model driven by SST reveals advantages, as it reveals teleconnections within the climate system, which connect source and target areas over long distances. Coupled atmosphere and ocean model approaches are here at a disadvantage, as they do not allow for the prescription of certain forcing fields. They are much more in advantage when discussing the impact and consequence of climate modes.

From our model study, investigating probable sources

of multidecadal variability over the North Atlantic, we conclude that multidecadal variability in the North Atlantic realm consists of two components of different time scale, a signal at about 60-70 years period which is of Atlantic origin and obvious in both SAT and SLP (ATL experiment). Although not derived from our model approach, this component is most likely associated with the Atlantic thermohaline circulation (e.g. Latif et al., 2004), because the atmospheric field (SLP) follows closely the oceanic surface quantity (SST). The second component of the Atlantic multidecadal variation has a period of about 80-100 years and is connected to the PNA pattern, as indicated in the experiment with Pacific only forcing. The separation between different sources for Atlantic multidecadal variability, found in our study, with contributions from different ocean basins enables the opportunity for an extended analysis of this climate mode. This also has implications when discussing predictability on decadal to multidecadal time scales (Latif et al., 2006). While the impact of the Atlantic Ocean on the long-term multidecadal variability is accepted, the mechanisms behind the multidecadal variability is not fully understood. Especially the contribution of different latitudes and ocean basins are still highly controversial. Hence, our simplified linear approach for the interpretation of the different time scales and impacts can therefore be regarded as a hypothesis which has to be further investigated with conceptual models as well as high resolution coupled ocean-atmosphere modeling efforts.

6 Acknowledgments

This work has been funded by the German Federal Ministry of Education and Research through DEKLIM project "Climate Transitions". The Kaplan et al. SST data are provided by the NOAA-CIRES Climate Diagnostics Centre, Boulder, Colorado, USA. The authors are grateful to F. Lunkeit and K. Fraedrich, Institute for Meteorology, Hamburg, making the most recent PUMA code available. We thank two anonymous reviewers for their constructive and helpful comments.

Appendix

To emphasize the model behavior for the 20 ensemble members and to identify regions of high and low atmospheric variability as response to global SST forcing, we investigate the atmospheric response pattern to SST-initial conditions in ensemble simulations. This can be used to quantify the random component of internal variability, where as the relative similarity between single ensemble members quantifies the potentially predictable component of the variance. A standard statistic tool for this kind of analysis is the "analysis of variance" (ANOVA), in which the total atmospheric variance (σ_{tot}^2) of a time-averaged quantity is separated into two components, one due to oceanic (SST) forcing (σ_{sst}^2), and the other component due to random internal variability σ_{int}^2 (e.g. Rowell, 1998; von Storch and Zwiers, 1999). Potential predictability is then measured as the ratio of ocean-forced variance to total variance ($\sigma_{sst}^2/\sigma_{tot}^2 * 100$) with values between 0%-100%. Hence, in regions where the ratio is large, we can assume that the influence of time-varying SST dominates over internal atmospheric variability. For signif-

icance testing, a Fisher's F test is performed, according to the criteria, that ocean forcing has no impact on simulated internal climate variability (Rowell, 1998). Considering that the running mean filter reduces the degrees of freedom of the full integration time to $(145/21=)$ 7 and taking into account the number of ensembles, the significance of ANOVA is calculated at 95% confidence level.

As expected, high variance ratios for DJF SAT are found overall ocean regions (Fig. 14a) while land surfaces depict lower values, a direct response to SST forcing. Especially in the tropics, SST has a strong impact with high potential predictability. Over land, internal variability becomes more important induced by higher variability between single ensemble members than over the ocean, leading to lower ratios. Nevertheless, except for the Antarctic belt, the oceanic forcing has a statistical significant and, therefore, predictable influence all over the globe on multidecadal time scales. Compared for example to Pohlmann et al. (2004), variance in the Southern Ocean SST variability is reduced and not significant with respect to 95% confidence interval. The reason is most probably due to the sparse Kaplan et al. (1998) data coverage in time and space over the Southern Ocean. The anomaly SST data is superposed onto the global SST climatology (Rayner et al., 1996), which then leads to only weak variability. In addition, our estimations are focused on the winter (DJF) season, where atmospheric teleconnections in the Northern Hemisphere are strongest, but in the Southern Hemisphere might be smallest (summer).

For SLP (Fig. 14b), highest variance ratios are found over the tropics, reflecting high persistence of SLP patterns and strong SST impact on the atmospheric response as suggested by Hoerling et al. (2001). Over the Atlantic, low variance ratios and hence increased non-stationary between the ensemble members is detected over South Greenland, the Labrador Sea, and north-eastern Europe. Increased ratios (up to 38%) can be found over central and eastern North America, possibly due to Pacific-Atlantic teleconnections. In the north-western Pacific, high ratios are possible due to teleconnection within the multidecadal mode as suggested by Delworth and Mann (2000) for this region. In general, the SLP structure has much more zonal character than for SAT, with increased potential predictability in the tropics and reduced but significant potential predictability in the extratropics. However, high variance ratios in SAT correspond to regions of high variance ratios in SLP, indicating the same source, namely SST. SLP at multidecadal time scales in high latitudes of both hemispheres is forced by other processes than ocean SST variability alone.

REFERENCES

- Bader, J. and Latif, M. 2003. The impact of decadal-scale Indian Ocean sea surface temperature anomalies on Sahelian rainfall and the North Atlantic Oscillation. *Geophys. Res. Lett.* **30**, 2169, doi:10.1029/2003GL018426.
- Barsugli, J. J. and Battisti, D. S. 1998. The basic effect of atmosphere-ocean thermal coupling on midlatitude variability. *J. Atmos. Sci.* **55**, 477-493.
- Bjerknes, J. 1964. Atlantic air-sea interaction. *Adv. Geophys.* **10**, 1-82.
- Bretherton, C. S. and Battisti, D. S. 2000. An interpretation of th

- results from atmospheric general circulation models forced by the time history of the observed sea surface temperature distribution. *Geophys. Res. Lett.* **27**, 767-770
- Claussen, M., Mysak, L. A., Weaver, A. J., Crucifix, M., Fichefet, T., Loutre, M.-F., Weber, S. L., Alcamo, J., Alexeev, V. A., Berger, A., Calov, R., Ganopolski, A., Goosse, H., Lohmann, G., Lunkeit, F., Mokhov, I. I., Petoukhov, V., Stone, P. and Wang, Zh. 2002. Earth System models of intermediate complexity: Closing the gap in the spectrum of climate system models. *Clim. Dyn.* **18**, 579-586.
- Crowley, T. J. 1992. North Atlantic deep water cools the Southern Hemisphere. *Paleoceanogr.* **7**, 489-497.
- Dima, M., and G. Lohmann 2007. A mechanism for the Atlantic multidecadal variability. *J. Clim.*, **20**, 11, 2706-2719.
- Delworth, T. L. and Mann, M. E. 2000. Observed and simulated multidecadal variability in the Northern Hemisphere. *Clim. Dyn.* **16**, 661-676.
- Deser, C. and Blackmon, M. 1993. Surface climate variations over the North Atlantic ocean during winter: 1900-1989. *J. Clim.* **6**, 1743-1753.
- Dickson, R. R., Meincke, J., Malmberg, S.-A. and Lee, A. J. 1988. The 'Great Salinity Anomaly' in the northern North Atlantic 1968-1982. *Prog. Oceanogr.* **20**, 103-151.
- Dong, B., Sutton, R. T. and Scaife, A. A. 2006. Multidecadal modulation of El Niño-Southern Oscillation (ENSO) variance by Atlantic sea surface temperatures. *Geophys. Res. Lett.* **33** L08705, doi:10.1029/2006GL025766.
- Enfield, D. B., Mestas-Nunez, A. M. and Trimble, P. J. 2001. The Atlantic multidecadal oscillation and its relation to rainfall and river flows in the continental U.S. *Geophys. Res. Lett.* **28**, 2077-2081.
- Folland, C. K., Karl, T. R., Christy, J. R., Clarke, R. A., Gruza, G. V., Jouzel, J., Mann, M. E., Oerlemans, J., Salinger, M. J. and Wang, S. W. 2001. Observed climate variability and change. In: *Climate Change 2001. The scientific basis. Contribution of working group I to the Third Assessment Report of the Intergovernmental Panel on Climate Change* (eds Houghton, J. T., Ding, Y., Griggs, D. J., Noguer, M., van der Linden, P. J., Dai, X., Maskell, K. and Johnson, C. A.). Cambridge University Press, United Kingdom and New York, NY, USA, 881pp.
- Fraedrich, K., Kirk, E. and Lunkeit, F. 1998. Portable University Model of the Atmosphere. *Deutsches Klimarechenzentrum, Tech. Rep.* **16**, 37pp, [Available online at <http://www/dkrz.de/forschung/reports.html>].
- Fraedrich, K., Kirk, K., Luksch, U. and Lunkeit, F. 2005. The Portable University Model of the Atmosphere (PUMA): Storm track dynamics and low frequency variability. *Meteorol. Zeitschrift* **14**, 735-745.
- Greatbatch, R. J., Lu, J. and Peterson, A. 2004. Nonstationary impact of ENSO on Euro-Atlantic winter climate. *Geophys. Res. Lett.* **31**, L02208, doi:10.1029/2003GL018542.
- Gray, T. G., Betancourt, J. L., Fastie, C. L. and Jackson, S. T. 2003. Patterns and sources of multidecadal oscillations in drought-sensitive tree-ring records from the central and southern Rocky Mountains. *Geophys. Res. Lett.* **30**, doi:10.1029/2002GL016154.
- Grosfeld, K., Lohmann, G., Rambu, N., Fraedrich, K. and Lunkeit, F. 2007. Atmospheric multidecadal variations in the North Atlantic realm: proxy data, observations, and atmospheric circulation model studies. *Clim Past* **3**, 39-50.
- Hoerling, M., Hurrell, J. W. and Xu, T. 2001. Tropical origins for recent North Atlantic climate change. *Science* **292**, 90-92.
- Hoskins, B. J. and Simmons, A. J. 1975. A multi-layer spectral model and the semi-implicit method. *Q. J. R. Meteorol. Soc.* **101**, 637-655.
- Hoyt, D. V. and Schatten, K. H. 1997. The role of the sun in climate change. *Oxford Univ Press*, New York, 275 pp.
- Hurrell, J. W. 1995. Decadal trends in the North Atlantic Oscillation: regional temperature and precipitation. *Science* **269**, 676-679.
- Hurrell, J. W. 1996. Influence of variations in extratropical winter-time teleconnections on Northern Hemisphere temperature. *Geophys. Res. Lett.* **23** 665-668.
- IPPC, 2001. *Climate Change 2001: The Scientific Basis. Contribution of working group I to the Third Assessment Report of the Intergovernmental Panel on Climate Change* (eds Houghton, J. T., Ding, Y., Griggs, D. J., Noguer, M., van der Linden, P. J., Dai, X., Maskell, K. and Johnson, C. A.). Cambridge University Press, United Kingdom and New York, NY, USA, 881pp.
- James, I. N. and James, P. M. 1989. Ultra-low-frequency variability in a simple atmospheric model. *Nature* **342**, 53-55.
- Jungclauss, J. H., Haak, H., Latif, M. and Mikolajewicz, U. 2000. Arctic-North Atlantic interactions and multidecadal variability of the meridional overturning circulation. *J. Clim.* **18**, 4013-4031, DOI: 10.1175/JCLI3462.1.
- Kaplan, A., Cane, M. A., Kushnir, Y., Clement, A., Blumenthal, M. and Rajagopalan, B. 1998. Analyses of global sea surface temperature 1856-1991. *J. Geophys. Res.* **103**, 567-589.
- Kaplan, A., Kushnir, Y., Cane, M. A. 2000. Reduced space optimal interpolation of historical marine sea level pressure. *J. Clim.* **13**, 2987-3002.
- Kerr, R. 2000. A North Atlantic climate pacemaker for the centuries. *Science* **288**, 1984-1986.
- Knight, J. R., Allan, R. J., Folland, C. K., Vellinga, M. and Mann, M. E. 2005. A signature of persistent natural thermohaline circulation cycles in observed climate. *Geophys. Res. Lett.* **32**, L20708, doi:10.1029/2005GL024233.
- Kuo, H. L. 1965. On formation and intensification of tropical cyclones through latent heat release by cumulus convection. *J. Atmos. Sci.* **22**, 40-63.
- Kuo, H. L. 1974. Further studies of the parameterization of the influence of cumulus convection on large-scale flow. *J. Atmos. Sci.* **31**, 1232-1240.
- Kushnir, Y. 1994. Interdecadal variations in North Atlantic sea surface temperature and associated atmospheric conditions. *J. Clim.* **7**, 141-157.
- Latif, M., Arpe, K., and Roeckner, E. 2000. Oceanic control of decadal North Atlantic sea level pressure variability in winter. *Geophys. Res. Lett.* **27**, 727-730.
- Latif, M., Roeckner, E., Botzet, M., Esch, M., Haak, H., Hagemann, S., Jungclauss, J., Legutke, S., Marsland, S., Mikolajewicz, U. and Mitchell, J. 2004. Reconstructing, monitoring, and predicting multi-decadal-scale changes in the North Atlantic thermohaline circulation with sea surface temperature. *J. Clim.* **17**, 1605-1614.
- Latif, M., Collins, M., Pohlmann, H. and Keenlyside, N. 2006. A review of predictability studies of Atlantic sector climate on decadal time scales. *J. Clim.* **19**, 5971-5987.
- Lohmann, G., Rambu, N. and Dima, M. 2004. Climate signature of solar irradiance variations: Analysis of long-term instrumental and historical data. *Int. J. Clim.* **24**, 1045 - 1056, doi: 10.1002/joc.1054.
- Luterbacher, J., Xoplaki, E., Dietrich, D., Rickli, R., Jacobeit, J., Beck, C., Gyalistras, D., Schmutz, C. and Wanner, H. 2002. Reconstruction of Sea Level Pressure fields over the Eastern North Atlantic and Europe back to 1500. *Clim. Dyn.* **18**, 545-561.
- Mann, M. E., Bradley, R. S. and Hughes, M. K. 1998. Global-scale temperature patterns and climate forcing over the past six centuries. *Nature* **392**, 779-787.
- Mann, M. E. and Park, J. 1999. Oscillatory spatiotemporal signal detection in climate studies: a multiple-taper spectral domain approach. *Adv. Geophys.* **41**, 1-131.
- Mehta, V. M., Suarez, M. J., Manganello, J. and Delworth, T. L.

2000. Ocean influence on the North Atlantic Oscillation and associated Northern Hemisphere climate variations: 1959-1993. *Geophys. Res. Lett.* **27**, 121-124.
- Minobe, S. 1997. A 50-70 year climate oscillation over the North Pacific and over North America. *Geophys. Res. Lett.* **24**, 683-686.
- Pohlmann, H. and Latif, M. 2005. Atlantic versus Indo-Pacific influence on Atlantic-European climate. *Geophys. Res. Lett.* **32**, L05707, doi: 10.1029/2004GL021316.
- Pohlmann, H., Botzet, M., Latif, M., Roesch, A., Wild, M. and Tschuck, P. 2004. Estimating the long-term predictability potential of a coupled AOGCM. *J. Clim.* **17**, 4463-4472.
- Rayner, N. A., Horton, E. B., Parker, D. E., Folland, C. and Hackett, R. B. 1996. Version 2.2 of the Global sea-Ice and Sea Surface Temperature data set, 1903-1994. *Clim. Res. Tech. Note.* **74**, Hadley Centre, U.K. Meteorol. Off., Bracknell, England, 1996.
- Rimbu, N., Lohmann, G., Felis, T. and Pätzold, J. 2003. Shift in ENSO teleconnections as recorded by a Red Sea coral. *J. Clim.* **16**, 1414-1422.
- Rodwell M. J., Rowell, D. P. and Folland, C. K. 1999. Oceanic forcing of the wintertime North Atlantic Oscillation and European climate. *Nature* **398**, 320-323.
- Romanova, V., Lohmann, G., Grosfeld, K. and Butzin, M. 2006a. The relative role of oceanic heat transport and orography on glacial climate. *Quat. Sci. Rev.* **25**, 832-845, doi://10.1016/j.quascirev/2005.07.007.
- Rowell, D. P. 1998. Assessing potential seasonal predictability with an ensemble of multidecadal GCM simulation. *J. Clim.* **11**, 109-120.
- Saravanan, R. and McWilliams, J. C. 2001. Stochasticity and spatial resonance in interdecadal climate fluctuations. *J. Clim.* **16**, 849-862.
- Schlesinger, M. E. and Ramankutty, N. 1994. An oscillation in the global climate system of period 65-70 years. *Nature* **367**, 723-726.
- Schneider, E. K., Bengtsson, L. and Hu, Z.-Z. 2003. Forcing of Northern Hemisphere climate trends. *J. Atmos. Sci.* **60**, 1504-1521.
- Stenseth, N. C., Chan, K.-S., Tong, H., Boonstra, R., Boutin, S., Krebs, C. J., Post, E., O'Donoghue, M., Yoccoz, N. G., Forchhammer, M. C. and Hurrell, J. W. 1999. Common dynamic structure of Canada lynx populations within three climatic regions. *Science* **285**, 1071-1073.
- Sutton, R. T. and Hodson, D. L. R. 2003. Influence of the ocean on North Atlantic climate variability 1871-1999. *J. Clim.* **16**, 3296-3313.
- Thompson, D. W. J., Wallace, J. M., Hegerl, G. C. 2000. Annular modes in the extratropical circulation. Part II: Trends. *J. Clim.* **13**, 1018-1036.
- von Storch, H. and Zwiers, F. W. 1999. *Statistical Analysis in Climate Research* Cambridge University Press, Cambridge, UK, 484pp.
- Wallace, J. M. and Gutzler, D. S. 1981. Teleconnections in the geopotential height field during the Northern-Hemisphere winter. *Mon. Wea. Rev.* **109**, 784-812.
- Zhang, R., Delworth, T. L. and Held, I. M. 2007. Can the Atlantic Ocean drive the observed multidecadal variability in Northern Hemisphere mean temperature? *Geophys. Res. Lett.* **34**, L02709, doi:10.1029/2006GL028683.

Figure 1. Masking areas for experiments with prescribed SST forcing in the Atlantic (ATL) (medium grey) and Pacific (PAC) (dark grey). Land mask, as given by T21 resolution, is shaded light grey.

Figure 2. EOF analysis of global ensemble mean SAT derived from experiment GLOB. Prior to the analysis, the data were normalized and a 21 year running mean has been applied. Linear detrending was applied for (a,b,c). EOF1 explaining (a) 37% and (d) 60% of the variance. EOF2 explaining (b) 22% and (e) 15% of the variance. (c,d) Principal components for EOF1 (solid) and EOF2 (dashed).

Figure 3. Index of the North Atlantic (a) SAT and (b) SLP of 20 ensemble members of the PUMA simulation forced with global observed SST for the period 1856-2000 (Kaplan et al. 1998). All data are detrended, smoothed with a 21-year running mean filter prior to the analysis. Ensemble mean (c) SAT and (d) SLP index for the same regions in unfiltered and 21 years running mean filtered version indicates multidecadal modulation of inter-annual and decadal variability. In addition, indices based on observational data and reconstructions for SST (Kaplan et al., 1998; Mann et al., 1998) and SLP (Kaplan et al., 2000; Luterbacher et al., 2002) are shown for comparison.

Figure 4. Regression analysis of the SAT index as represented in Fig. 3a with the non-normalized field of the modeled ensemble mean SLP anomalous field. Light (dark) grey shading indicates positive (negative) values.

Figure 5. Time series of the first canonical modes for the globally forced atmospheric circulation experiment GLOB between (a) SAT and SLP, and (d) SAT and GPH500, respectively. Associated canonical modes for (b) SAT and (c) SLP, and (e) SAT and (f) GPH500. Maps of explained variance are underlayn in grey scale, indicating ranges (0-25%, 25-50%, 50-75%, 75-100%).

Figure 6. EOF analysis of global ensemble mean SAT derived from experiment ATL. Prior to the analysis, the data were detrended, normalized and a 21 year running mean has been applied. (a) Principal component for EOF1. The dotted line indicates the second EOF of experiment GLOB (comp. Fig. 2c). (b) EOF1 explaining 43% of the variance.

Figure 7. Time series of the first canonical modes for experiment ATL between (a) SAT and SLP, and (d) SAT and GPH500, respectively. Associated canonical modes for (b) SAT and (c) SLP, and (e) SAT and (f) GPH500. Maps of explained variance are underlayn in grey scale (compare Figure 5).

Figure 8. Index of North Atlantic (a) SAT and (b) SLP of 20 ensemble members for experiment ATL. Regression analysis of North Atlantic SAT and SLP indices with the non-normalized global ensemble mean (c) SAT and (d) SLP patterns. Prior to the analysis, the data were detrended and a 21 year running mean has been applied. Units are $^{\circ}C$ and hPa, respectively. Light (dark) grey shading indicates positive (negative) values.

Figure 9. EOF analysis of global ensemble mean SAT derived from experiment PAC. Prior to the analysis, the data were detrended, normalized and a 21 year running mean has been applied. (a) Principal component for EOF1. The dotted line indicates the first EOF of experiment GLOB (comp. Fig. 2c). (b) EOF1 explaining 53% of the variance.

Figure 10. Time series of the first canonical modes for the experiment PAC between (a) SAT and SLP, and (d) SAT and GPH500, respectively. The dotted line in (a) indicates an index of the PNA-like pattern as defined in the text, the dashed-dotted line represents the Niño3 index of ensemble mean SAT. Canonical modes for (b) SAT and (c) SLP, and (e) SAT and (f) GPH500, respectively. Grey scale indicates ranges of explained variance (compare Figure 5).

Figure 11. Index of North Atlantic (a) SAT and (b) SLP of 20 ensemble members for experiment PAC. Regression analysis of North Atlantic SAT and SLP indices with the non-normalized global ensemble mean (c) SAT and (d) SLP patterns. Prior to the analysis, the data were detrended and a 21 year running mean has been applied. Units are $^{\circ}C$ and hPa, respectively. Light (dark) grey shading indicates positive (negative) values.

Figure 12. Ensemble mean indices of North Atlantic SLP for averaging region ($90^{\circ}W-60^{\circ}W$; $25^{\circ}N-50^{\circ}N$).

Figure 13. Percentage variance of (a) SAT and (b) SLP due to oceanic SST forcing, computed from an ensemble of 20 members of the PUMA simulation for the period 1856 - 2000. Contour interval is 10%, white areas indicate values that do not exceed the 95% confidence interval, according to F-statistics. All data is detrended, smoothed with a 21-year running mean filter prior to the analysis.

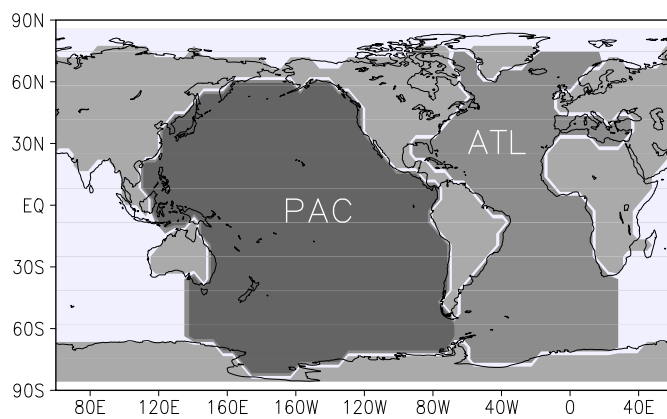


Figure 1: Masking areas for experiments with prescribed SST forcing in the Atlantic (ATL) (medium grey) and Pacific (PAC) (dark grey). Land mask, as given by T21 resolution, is shaded light grey.

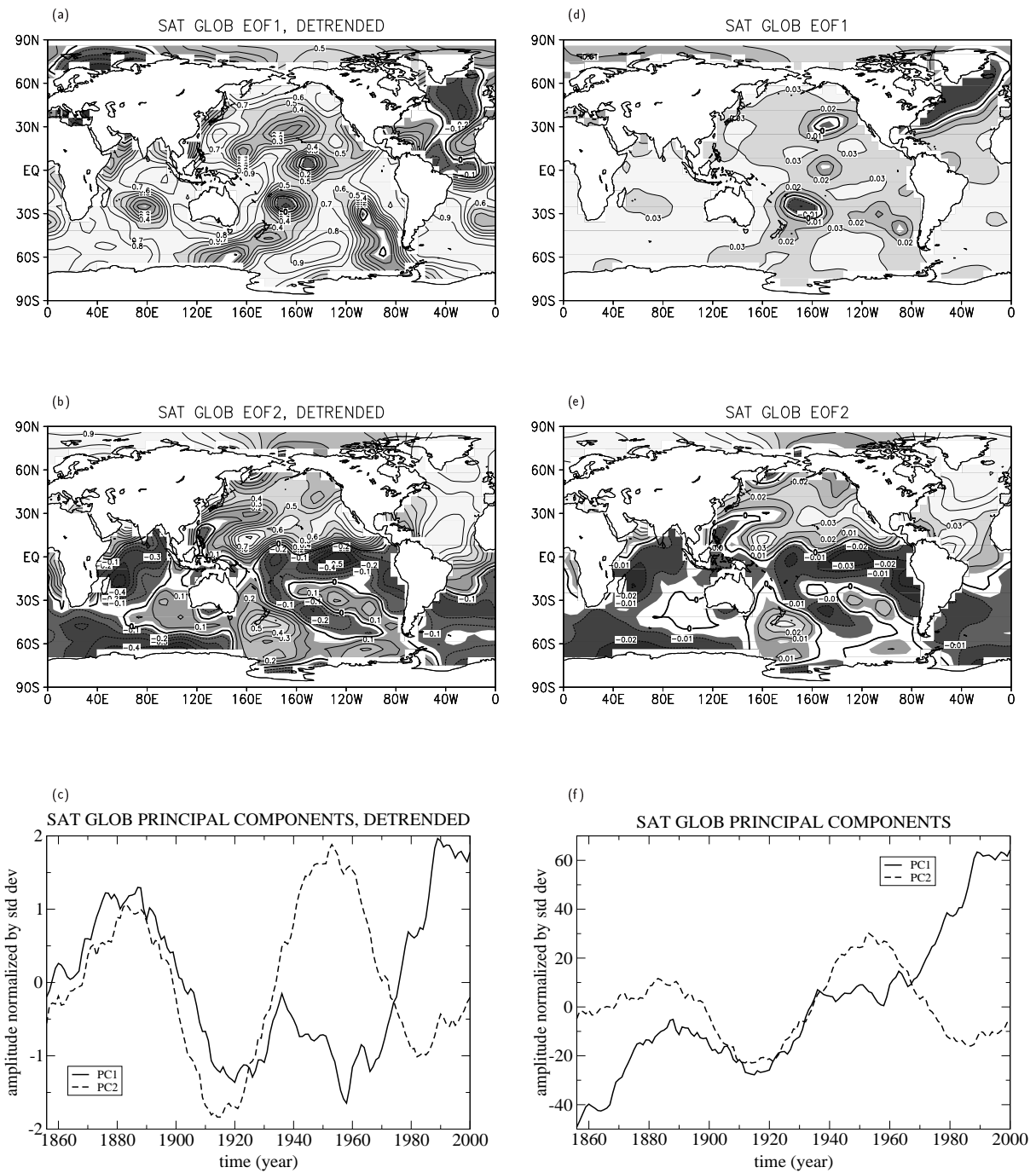


Figure 2: EOF analysis of global ensemble mean SAT derived from experiment GLOB. Prior to the analysis, the data were normalized and a 21 year running mean has been applied. Linear detrending was applied for (a,b,c). EOF1 explaining (a) 37% and (d) 60% of the variance. EOF2 explaining (b) 22% and (e) 15% of the variance. (c,d) Principal components for EOF1 (solid) and EOF2 (dashed).

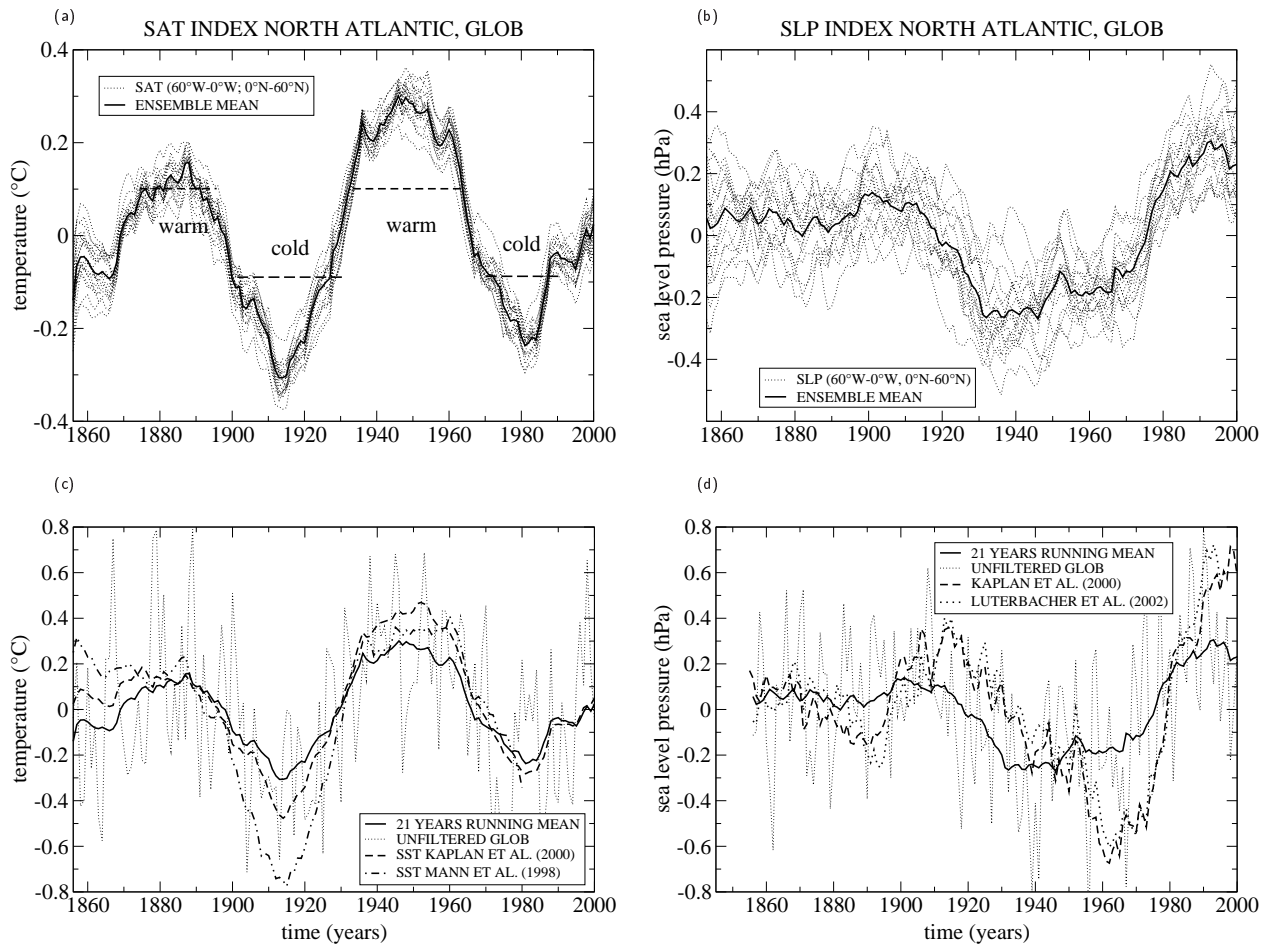


Figure 3: Index of the North Atlantic (a) SAT and (b) SLP of 20 ensemble members of the PUMA simulation forced with global observed SST for the period 1856-2000 (Kaplan et al. 1998). All data are detrended, smoothed with a 21-year running mean filter prior to the analysis. Ensemble mean (c) SAT and (d) SLP index for the same regions in unfiltered and 21 years running mean filtered version indicates multidecadal modulation of interannual and decadal variability. In addition, indices based on observational data and reconstructions for SST (Kaplan et al. 1998; Mann et al. 1998) and SLP (Kaplan et al. 2000; Luterbacher et al. 2002) are shown for comparison.

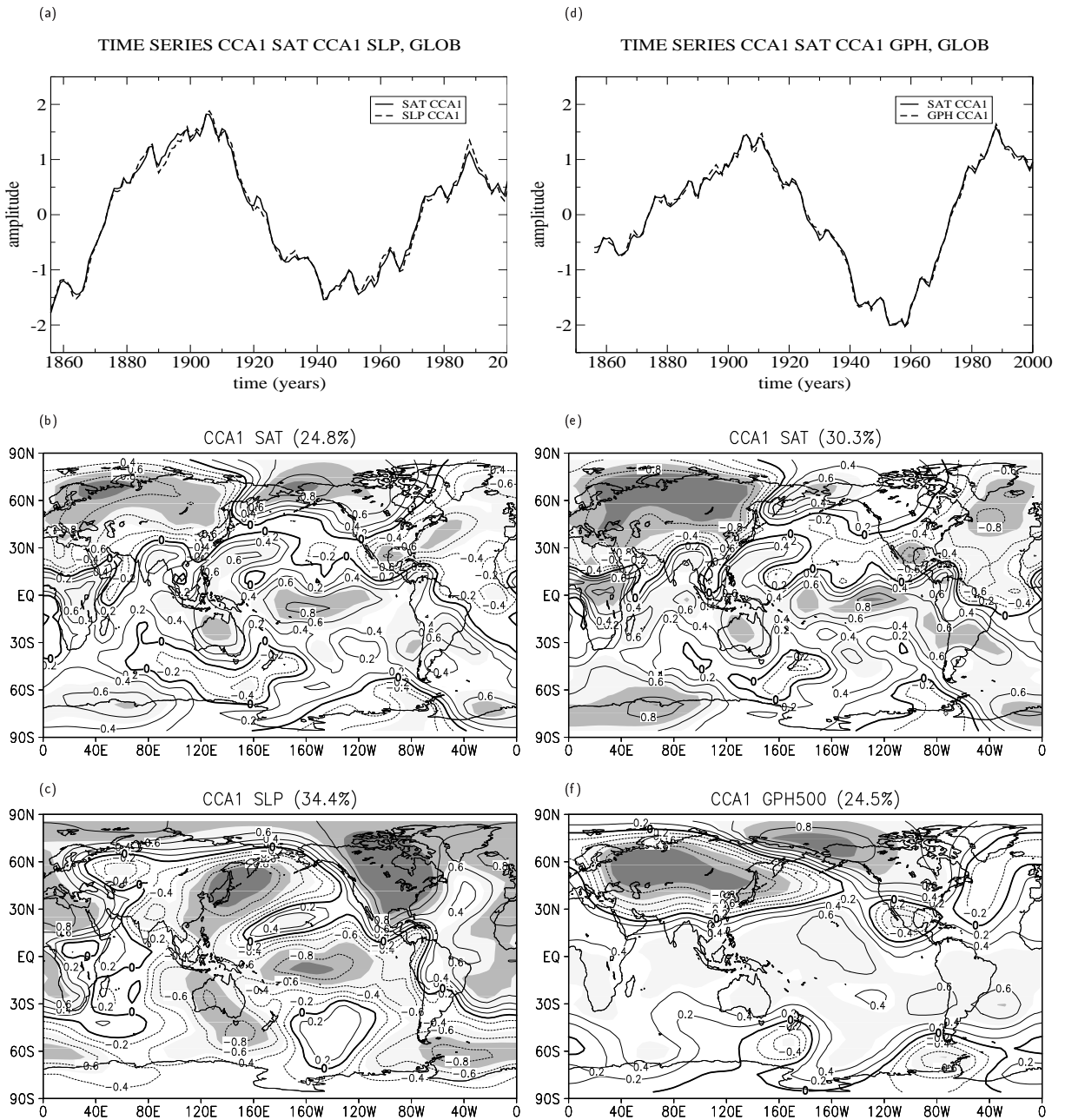


Figure 5: Time series of the first canonical modes for the globally forced atmospheric circulation experiment GLOB between (a) SAT and SLP, and (d) SAT and GPH500, respectively. Associated canonical modes for (b) SAT and (c) SLP, and (e) SAT and (f) GPH500. Maps of explained variance are underlain in grey scale, indicating ranges (0-25%, 25-50%, 50-75%, 75-100%).

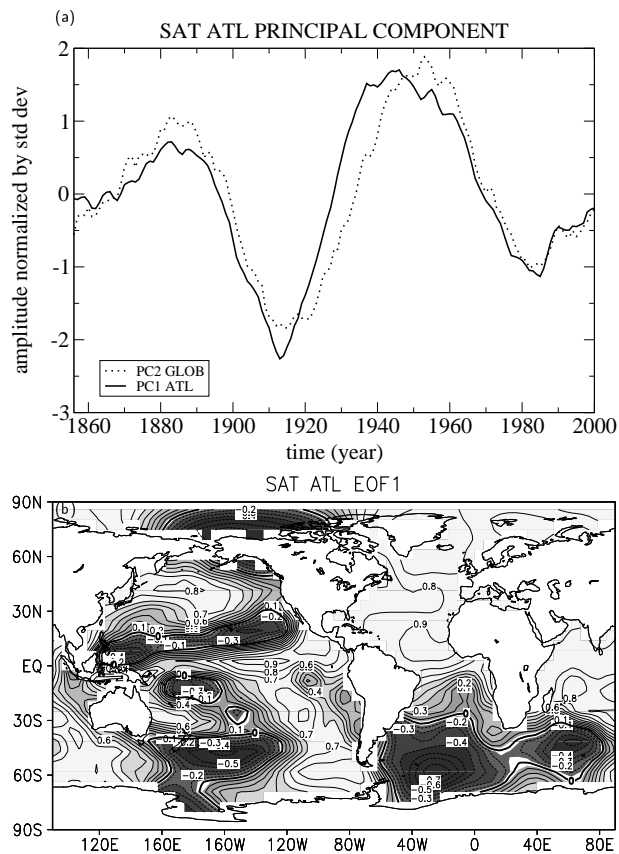


Figure 6: EOF analysis of global ensemble mean SAT derived from experiment ATL. Prior to the analysis, the data were detrended, normalized and a 21 year running mean has been applied. (a) Principal component for EOF1. The dotted line indicates the second EOF of experiment GLOB (comp. Fig. 2c). (b) EOF1 explaining 43% of the variance.

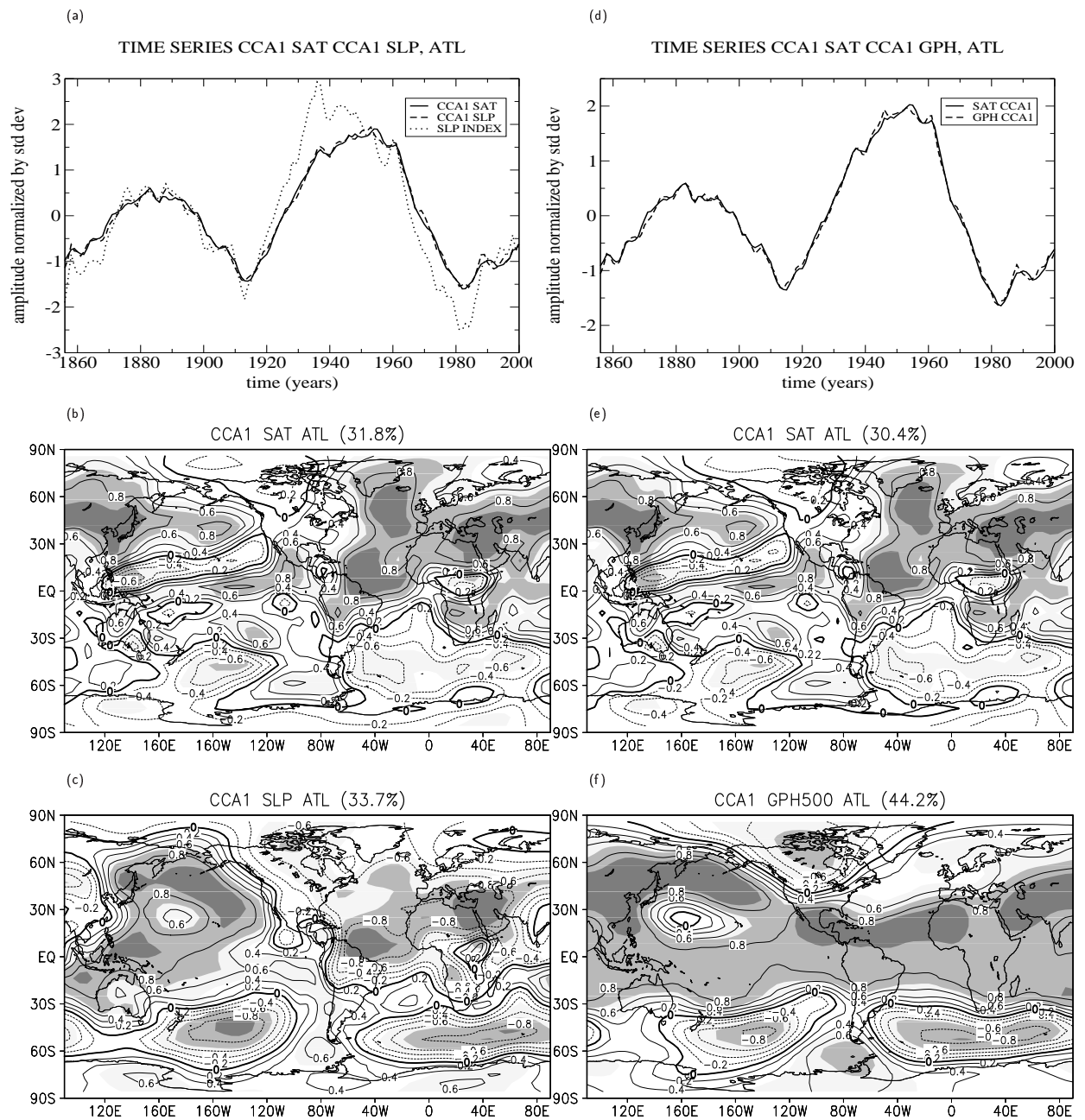


Figure 7: Time series of the first canonical modes for experiment ATL between (a) SAT and SLP, and (d) SAT and GPH500, respectively. Associated canonical modes for (b) SAT and (c) SLP, and (e) SAT and (f) GPH500. Maps of explained variance are underlain in grey scale (compare Figure 5).

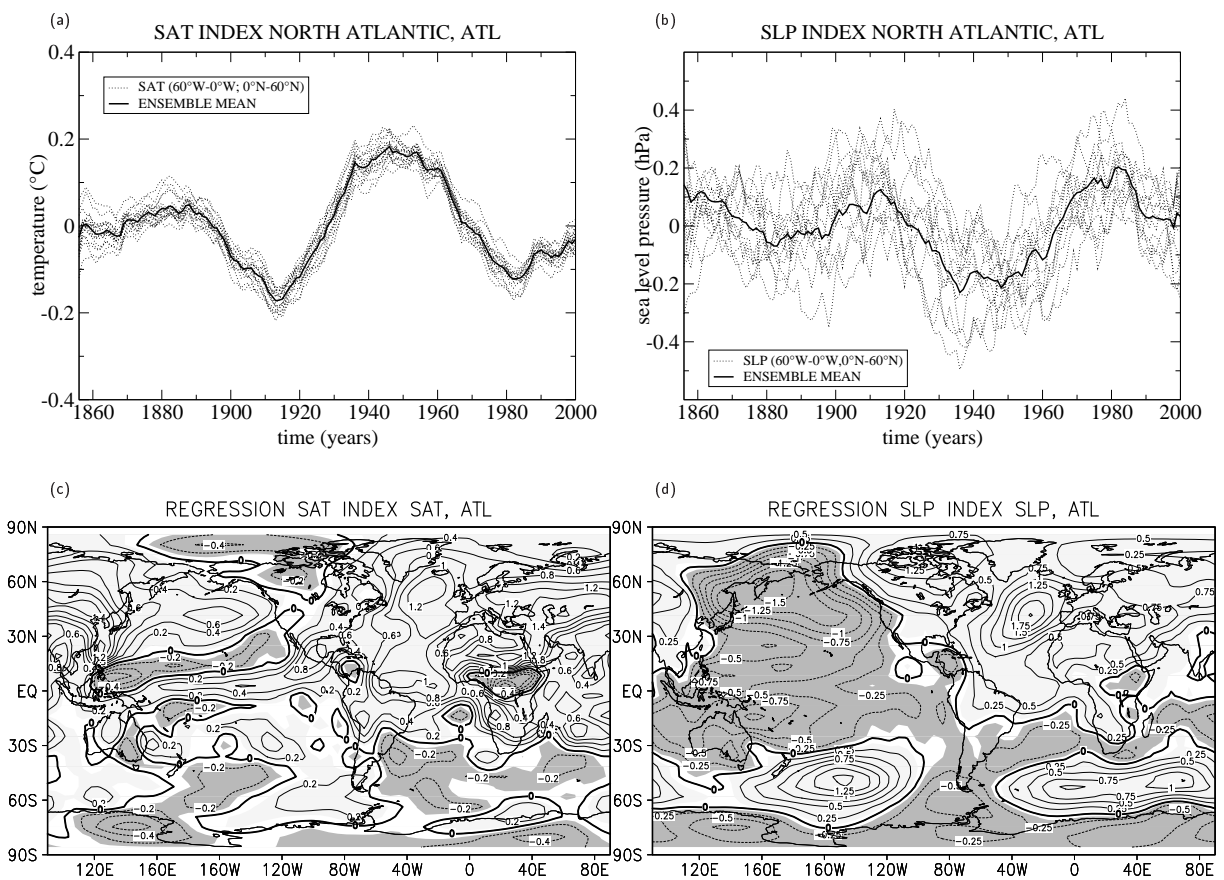


Figure 8: Index of North Atlantic (a) SAT and (b) SLP of 20 ensemble members for experiment ATL. Regression analysis of North Atlantic SAT and SLP indices with the non-normalized global ensemble mean (c) SAT and (d) SLP patterns. Prior to the analysis, the data were detrended and a 21 year running mean has been applied. Units are $^{\circ}\text{C}$ and hPa, respectively. Light (dark) grey shading indicates positive (negative) values.

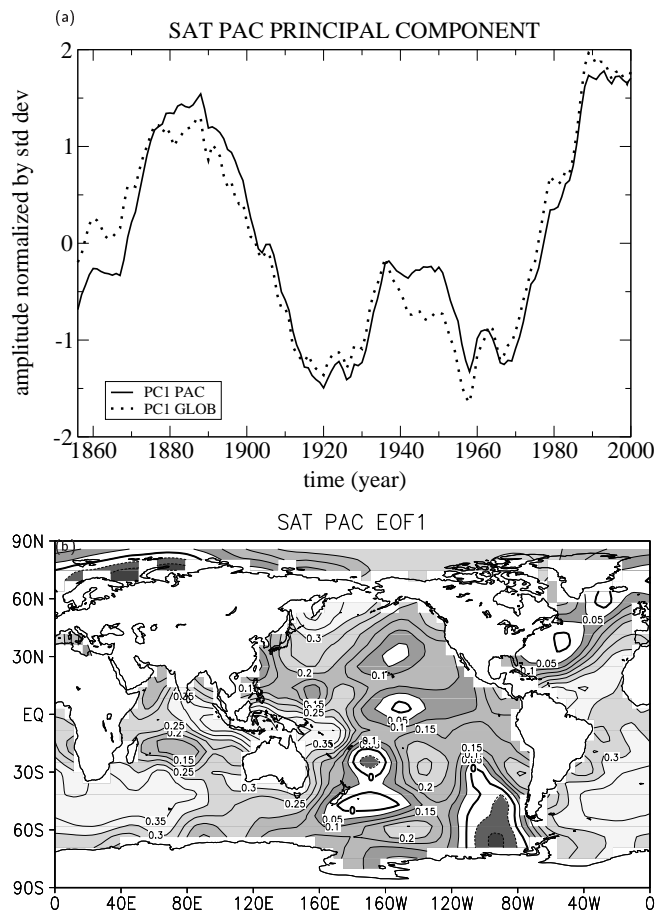


Figure 9: EOF analysis of global ensemble mean SAT derived from experiment PAC. Prior to the analysis, the data were detrended, normalized and a 21 year running mean has been applied. (a) Principal component for EOF1. The dotted line indicates the first EOF of experiment GLOB (comp. Fig. 2c). (b) EOF1 explaining 53% of the variance.

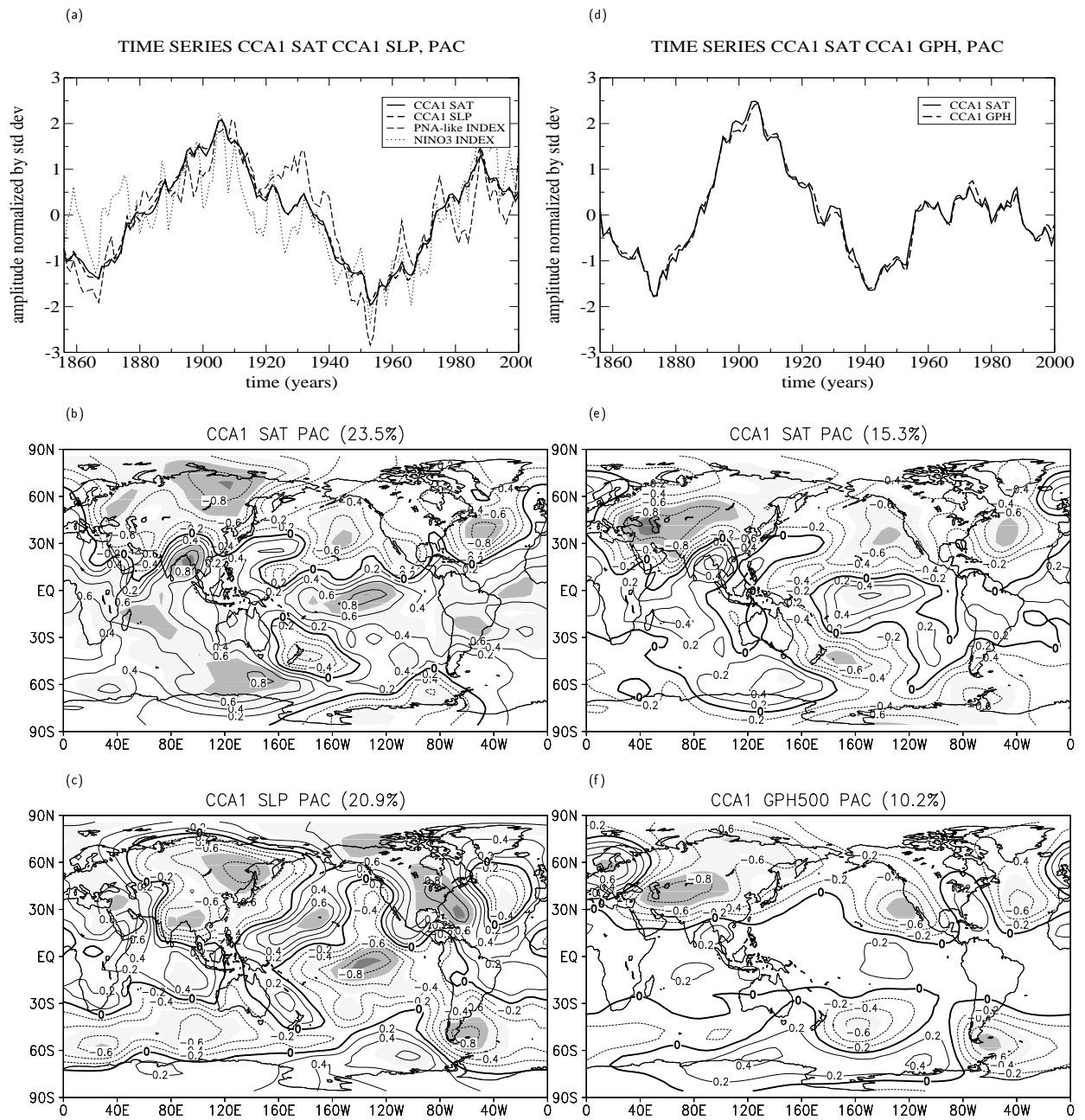


Figure 10: Time series of the first canonical modes for the experiment PAC between (a) SAT and SLP, and (d) SAT and GPH500, respectively. The dotted line in (a) indicates an index of the PNA-like pattern as defined in the text, the dashed-dotted line represents the Niño3 index of ensemble mean SAT. Canonical modes for (b) SAT and (c) SLP, and (e) SAT and (f) GPH500, respectively. Grey scale indicates ranges of explained variance (compare Figure 5).

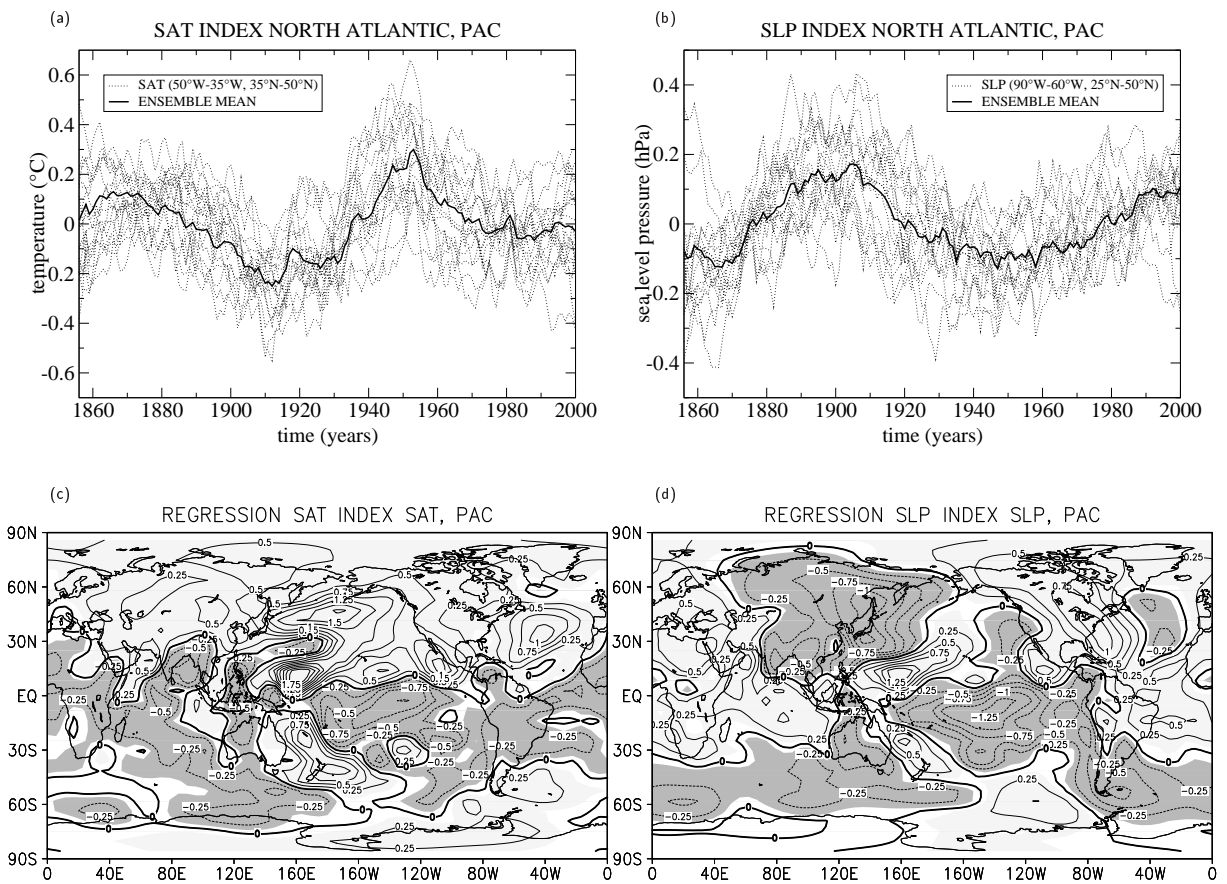


Figure 11: Index of North Atlantic (a) SAT and (b) SLP of 20 ensemble members for experiment PAC. Regression analysis of North Atlantic SAT and SLP indices with the non-normalized global ensemble mean (c) SAT and (d) SLP patterns. Prior to the analysis, the data were detrended and a 21 year running mean has been applied. Units are $^{\circ}\text{C}$ and hPa, respectively. Light (dark) grey shading indicates positive (negative) values.

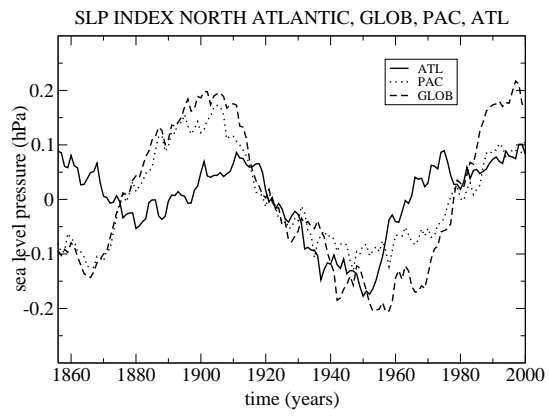


Figure 12: Ensemble mean indices of North Atlantic SLP for averaging region (90°W - 60°W ; 25°N - 50°N).

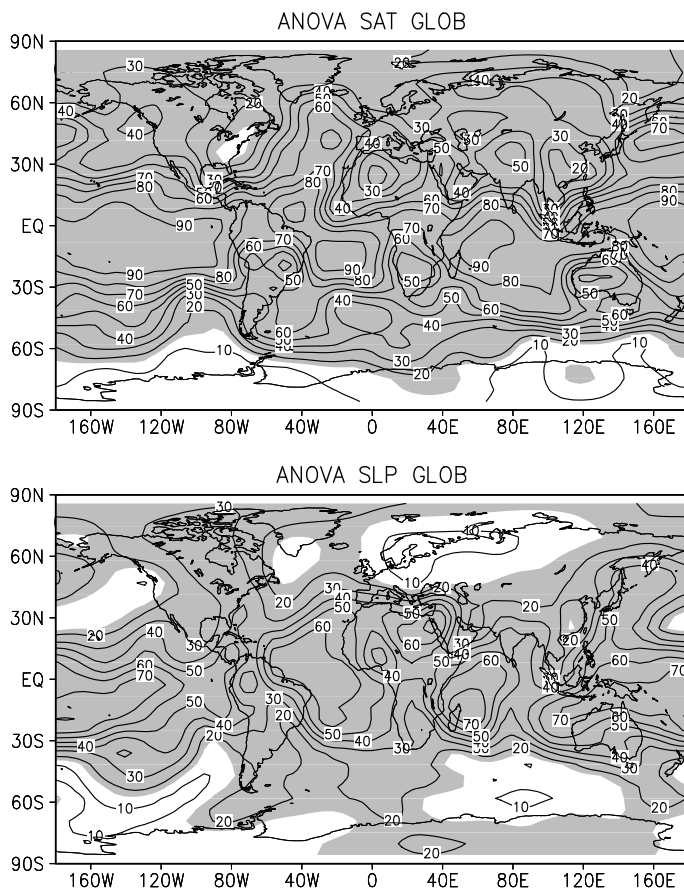


Figure 13: Percentage variance of (a) SAT and (b) SLP due to oceanic SST forcing, computed from an ensemble of 20 members of the PUMA simulation for the period 1856 - 2000. Contour interval is 10%, white areas indicate values that do not exceed the 95% confidence interval, according to F-statistics. All data is detrended, smoothed with a 21-year running mean filter prior to the analysis.